# Electric Field Modelling and Simulation of the High-voltage High-frequency Transformer Insulation Applied for Power Electronics Based on Circuit-field Coupling Analysis

Zhaoxin Wang; Claus Leth Bak; Filipe Faria da Silva; Henrik Sørensen
*Aalborg University, Aalborg, Denmark*

## Abstract

This paper established a transient electric field model of a high-voltage high-frequency (HVHF) transformer based on circuit-field coupling analysis. As the key component of power electronic transformers (PETs), the operating conditions of the HVHF transformer are determined by the converter circuit containing it. To find out the electrical stress withstood by the solid insulation, it is essential to model the transient electric field while considering the circuit model of the converter. The circuit model of the converter and the 3-D transient electric field model based on the finite element method (FEM) are built in ANSYS. The voltage and current waveforms on both primary and secondary sides of the HVHF transformer obtained from the converter model are coupled to the transient electric model as the excitations. Based on the established model, a case study of a 60 kHz HVHF transformer used for the dual active bridge (DAB) converter is investigated, and the electric field characteristics of the insulation are analyzed. The electric field distribution inside and on the surfaces of the insulation is present, and magnitude values of the highest electrical stress inside and on the surfaces of the insulation are identified. The theoretical verification is carried out based on the grid convergence index (GCI) method and it verifies the accuracy of the proposed model. This model could be used to calculate the overvoltage capacity of the HVHF transformers in various power electronics applications and it is an essential step in building the digital twin model of the HVHF transformer.

## 1. Introduction

Power electric transformers (PETs) or solid-state transformers (SSTs) provide an efficient and flexible solution for increasing the penetration of large-scale renewable energy such as solar power and wind power, due to their key roles in voltage conversion, electrical isolation, power transmission and control, and bidirectional energy flow [1-2]. As the component of the PET, the high-voltage high-frequency (HVHF) transformer has the advantages of compact size, high power density, and environmental friendliness with less material compared to traditional transformers. The reliability of the HVHF transformer is directly related to PETs safe and stable operation. The HVHF transformer normally operates with a non-sinusoidal wave voltage at high frequencies, which is determined by the topology of the converter. The insulation of the HVHF transformer suffers from high electrical stress for a long term, which has become one of the main contributors to its aging, failure, and breakdown [3-4]. However, the electrical stresses applied to the insulation are difficult to measure experimentally [5]. Studying the electric field distribution and insulation performance of the HVHF transformer is of great significance to its optimal design, condition monitoring, and lifetime prediction.

In recent decades, the finite element method (FEM) has been widely used to calculate the electric field of electrical equipment. Ref. [6] carried out the insulation design of the new printed-circuit board (PCB) technology medium voltage combined transformer using electric field analysis. The 3-D FEM numerical method is applied to compute the electric field distributions of the transformer to make sure that the permissible electric field strength for used materials was not exceeded in any part of the insulation system. Ref. [7] established the electric field model of a ±400 kV dry-type $SF_6$ gas insulated converter transformer bushing using the finite element analysis method. The electric field intensity distribution of the converter transformer bushing in SF6 gas under different voltages is analyzed. Ref. [8] simulated the electric field distribution of the converter transformer valve sidewinding in a practical ±800 kV converter transformer under polarity reversal test voltage. The simulations are carried out with different polarity reversal durations to analyze the influence of polarity reversal duration on the electric field distribution. Ref. [9] simulated the electric field of a 500 kV high voltage isolated energy supply transformer (HIET) for its insulation structure design. The electric field characteristics of the overall shielding structure are analyzed, and the results show that the electric field decreases with an increase in thickness of the insulation within a certain range, and the electric field reduction effect is weakened significantly when the thickness exceeds a threshold value. Ref. [10] established an electrothermal coupling model of an 800 kV converter transformer valve-side bushing using FEM. The electric field distribution of the valve-side bushing is investigated considering the influence of temperature, and the location of the maximum electric field strength is identified. However, the characteristics of electric field distribution and the electrical stress applied to the insulation for the HVHF transformer considering its actual working conditions are unclear, and further research is needed. This paper investigates the electrical stress withstood by the HVHF transformer from the

aspect of the converter and proposed a transient electric model based on the circuit-field coupling analysis.
In this paper, a geometrical model of a 60 kHz HVHF transformer is established first, and the parameters of it are given. Then, the converter model containing the HVHF transformer is introduced. Next, the theory of transient electric field analysis is described and the transient electric field model of the HVHF transformer is established. Finally, the electric field distribution characteristics of the insulation are present, and the electrical stress withstood by the insulation is investigated.

## 2. Geometrical model

The 3-D geometry of a 60 kHz HVHF transformer is built, as shown in Fig. 1, and its specifications are present in Table 1. To investigate the electrical stresses applied to the insulation, the solid insulation material is considered in the geometry model. For this model, the Nomex paper is used as the solid insulation between the layers of the windings. The physical properties of the materials used for the HVHF transformer are present in Table 2. To simplify the geometry model, the components that have little effect on the transient electric field analysis including base, tube, and bobbin are ignored.

**Table. 1** The specifications of the HVHF transformer

| Specification | Value |
|---|---|
| $V_{pri}/V_{sec}$ | 3.3 kV/3.3 kV |
| Frequency | 60 kHz |
| Turn ratio | 1:1 |
| Cooling type | Dry type |

**Table. 2** Material properties of the HVHF transformer

| Material | Relative permittivity | Bulk conductivity (S/m) |
|---|---|---|
| Ferrite LP3 | 12 | 0.01 |
| Copper | 1 | 145000 |
| Nomex paper | 2.4 | $1.67\times10^{-15}$ |
| Air | 1.000536 | $3\times10^{-15}$ |

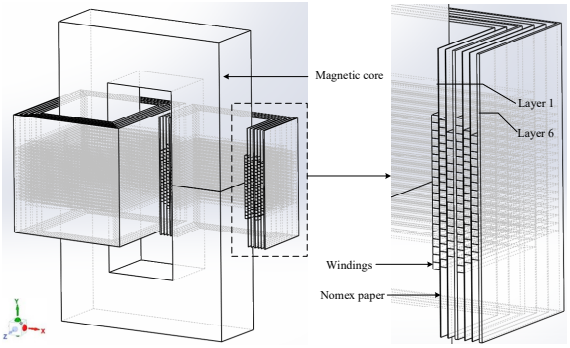


**Fig.** 1 The 3-D geometrical model of the HVHF transformer

## 3. Converter model

As the key component of PETs, HVHF transformers are often used to achieve voltage conversion and galvanic isolation. In fact, the voltage and current waveforms applied to the HVHF transformer are determined by the topology, parameters, and control method of the converter. To accurately investigate the electrical stresses applied to the insulation, it is essential to build the circuit model of the converter first to solve for the electrical parameters applied to the HVHF transformer.
The topology of a dual active bridge (DAB) DC-DC converter containing the HVHF transformer is given in Fig. 2. The DAB DC-DC converter is usually used for the PETs applications due to its wide voltage regulation and ability to achieve soft switching over a wide range of loading [11]. The application of the HVHF transformer could significantly increase the power density and modularity of the converter.

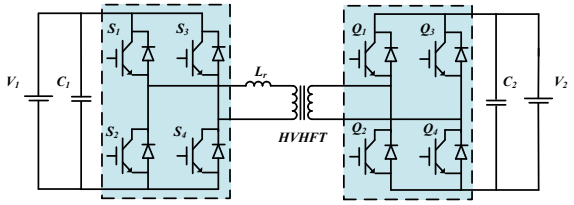


**Fig. 2** The topology of the DAB converter model

The AC sides of the two full-bridge converters are connected by an inductor and a HVHF transformer. Each full-bridge converter generates a high-frequency square wave voltage on the AC side. The magnitude and direction of power flow can be adjusted by changing the phase shift between the two AC sources.
In this case, the phase shift control method is applied for the DAB converter. The switching frequency of the full-bridge circuits on both sides is 60 kHz. The conduction angle of switches is set to 180° to generate a square wave voltage with a duty cycle (the percentage of the ratio of pulse duration to the total period of the waveform) of 50 %. The minimum and maximum time step of the simulation is set to 0.1 µs and 1 µs respectively. The simulation time is set to 150 µs.
In this research, the ANSYS Simplorer is employed to solve the DAB converter model.

## 4 Transient electric field model

The transient electromagnetic field of the HVHF transformer is governed by Maxwell's equations, which are shown as (1)-(4)

$$\nabla \cdot \boldsymbol{E} = \frac{\rho}{\varepsilon_0} \tag{1}$$

$$\nabla \cdot \boldsymbol{B} = 0 \tag{2}$$

$$\nabla \times \boldsymbol{E} = -\frac{\partial \boldsymbol{B}}{\partial t} \tag{3}$$

$$\nabla \times \boldsymbol{B} = \mu_0 \boldsymbol{J} + \mu_0 \varepsilon_0 \frac{\partial \boldsymbol{E}}{\partial t} \tag{4}$$

where $E$ is the electric field strength vector, $B$ is magnetic flux density vector, $J$ is the current density vector, $\rho$ is the charge density, $\mathcal{E}_0$ is the permittivity of the vacuum, and $\mu_0$ is the permeability of the vacuum.
To solve the transient electromagnetic field using FEM, the electrical voltage $V$ ie introduced, which ie defined by (5)

$$\boldsymbol{E} = -\nabla V \tag{5}$$

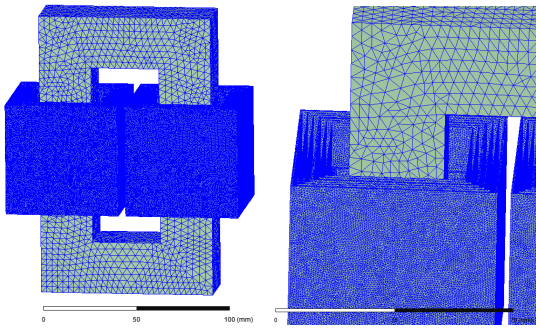

**Fig. 3** Meshing results

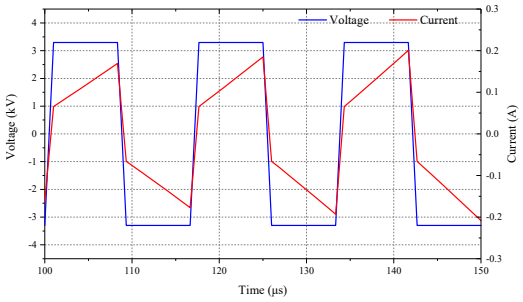


a. Primary windings

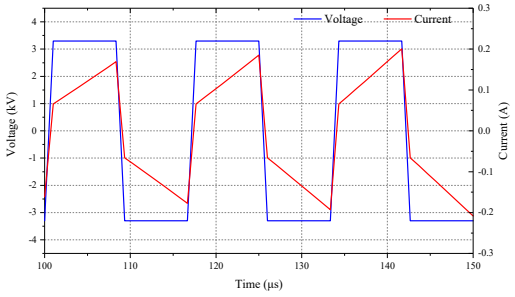


b. Secondary windings

**Fig. 4** Voltage and current waveforms applied to the HVHF transformer

The transient electric field equations could be derived with the boundary condition as (6) and (7)

$$\nabla\left(\varepsilon\frac{\partial}{\partial t}+\sigma\right)\nabla V=0 \tag{6}$$

$$V\big|_{\Gamma_D}=u(t) \tag{7}$$

Where $\mathcal{E}$ is the permittivity, σ is electrical conductivity. Considering both the accuracy and time cost of the simulation model, the tetrahedral meshing method is applied to divide the computational domain. The grid length is set to 4.5 mm, 0.6 mm, 0.6 mm, and 35 mm for the magnetic core, windings, Nomex paper, and air region respectively. The mesh results are shown in Fig. 3. The grid convergence index (GCI) method is used to make sure the mesh is divided sufficiently. The mesh validation process and results will be present in section 6. The time step is set to 1 μs, and the simulation is set to 150 μs.

The ANSYS Maxwell based on FEM is applied to solve the transient electric field model of the HVHF transformer.

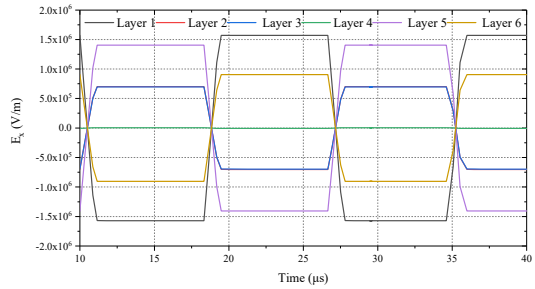


a. The maximum electric field strength in the x-direction

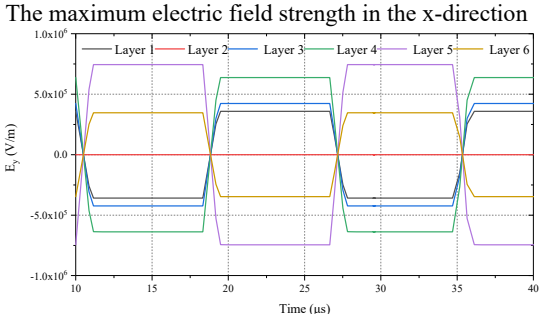


b. The maximum electric field strength in the y-direction

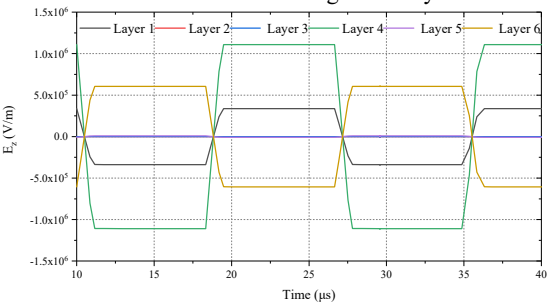


c. The maximum electric field strength in the z-direction

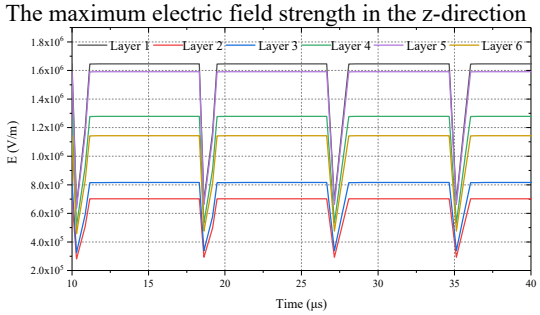


d. The maximum magnitude of the electric field strength

**Fig. 5** The maximum electric field strength in the 6 layers of the insulation

## 5. Simulation results

### 5.1 Converter model

According to the established model, the voltage and current waveforms applied to both sides of the HVHF transformer in the DAB converter under the rated condition are present in Fig. 4. The simulation results are coupled to the primary and secondary windings in the transient electric model as the excitation to evaluate the electrical characteristics of the insulation.

### 5.2 Transient electric field model

The layout of the windings and the core affects the electric field distribution of the insulation. For the HVHF transformer model studied in this paper, the simulation

results show that the insulation for the primary and secondary windings withstands the same electrical stresses due to its structure being symmetrical about the yz-plane. Therefore, only the electric field results of the insulation for the primary windings are analyzed in this section.

Fig. 5 represents the curves of the maximum electric field strength in the 6 layers of the insulation with the time. It is indicated that, each layer of the insulation is subjected to different electric stresses in *x*, *y*, and *z* directions (the directions are given in Fig. 1). The 1st, 5th, and 4th layers of the insulation withstand the maximum electric field strength in the *x*, *y*, and *z* directions respectively. The 1st layer of the insulation withstands the highest electric field strength with a magnitude value is 1.65 kV/mm. The dielectric strength of the Nomex paper considered in this model is 33.5 kV/mm, which means there is no threat of insulation breakdown for the HVHF transformer under the current working condition.

To investigate the electric field distribution characteristics on the surfaces of the insulation at different moments, the simulation results at different moments of $t_1$, $t_2$, and $t_3$ are present in Fig. 6. The electric field distribution shows a similar characteristic at different moments in a period. It is found that the electric field on the surfaces of the insulation is concentrated at both ends of the windings. The magnitude of the maximum electric field on the insulation surfaces is 1.25 kV/mm, which is lower than the electric field strength that partial discharges (PD) start to occur (2.66 kV/mm) [12]. It means that there is no threat of PD occurring on the insulation under the current operating condition. However, the surfaces of the insulation are assumed to be ideally smooth in the simulation. The insulation's level of pollution will influence the threshold electric field strength, which needs to be considered in reality.

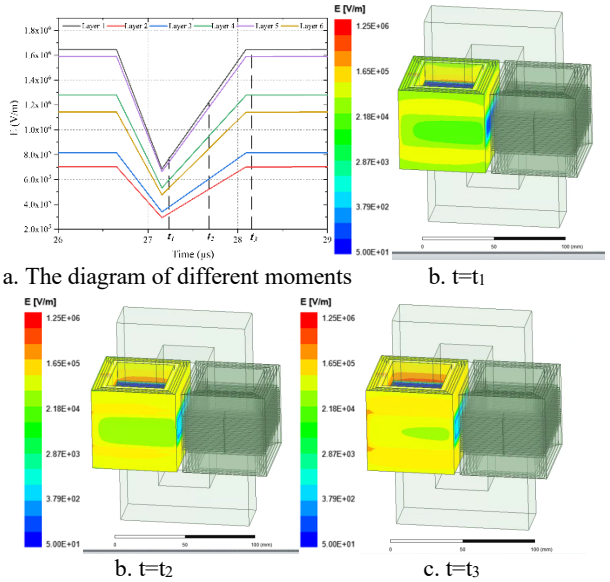


a. The diagram of different moments b. t=$t_1$

b. t=$t_2$ c. t=$t_3$

**Fig.** 6 The electric field distribution on the surfaces of the insulation at different moments

The electric field distribution for each layer of the insulation at $t_3$ is shown in Fig. 7. It is found that at the same moment, the electric field distribution shows similar characteristics for each layer. The electric field strength near the end of the winding is high, resulting in each layer of the insulation withstanding large electric field stress near the end of the winding. The maximum electric field strength appears on the 1st layer of the insulation. The maximum electric field strength values for each layer on the surfaces of the insulation at $t_3$ are shown in Table 3. It can be seen in Table 3 that, the maximum electric field decrease from layer 1 to layer 2, and then increase from layer 2 to layer 6. The maximum electric field strength from layer 1 to layer 6 does not vary linearly because of the structure of the windings. The difference in the lengths of each layer of the windings result in a significantly uneven distribution of the electric field in the insulation near the ends of the windings, as shown in Fig. 8. To find out the position that withstands the highest electrical stress, the electric field distribution was calculated and plotted along 6 lines on the surfaces of the insulation, as shown in Fig. 10. The diagram of the lines is present in Fig. 9. The results show that the magnitude value of the electric field strength for each layer decreases from the position near the ends of the windings towards the ends of the insulation and reaches a maximum near the ends of the windings.

**Table. 3** The maximum electric field strength for each layer

| Layer | 1 | 2 | 3 |
|---|---|---|---|
| E field (kV/mm) | 1.25 | 0.63 | 0.65 |
| Layer | 4 | 5 | 6 |
| E field (kV/mm) | 0.65 | 1.12 | 1.13 |

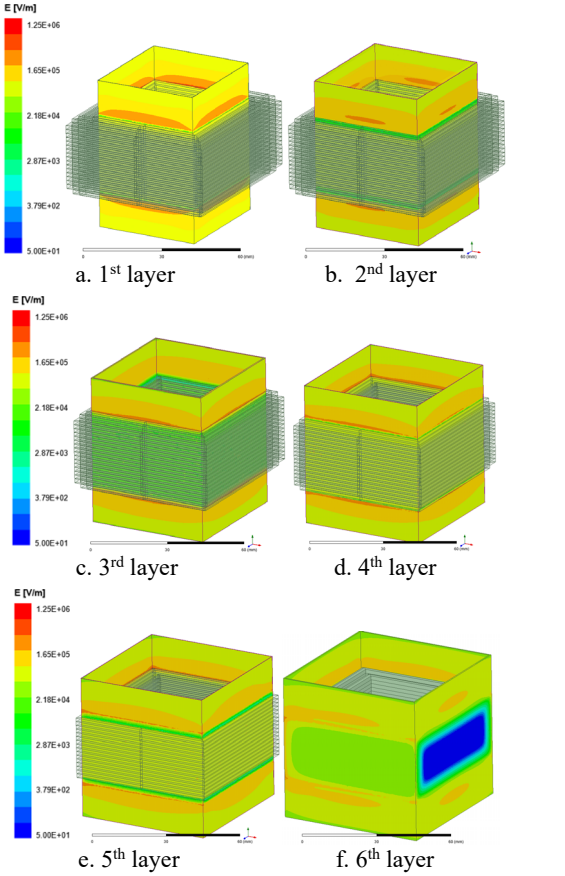


a. 1st layer b. 2nd layer

c. 3rd layer d. 4th layer

e. 5th layer f. 6th layer

**Fig. 7** The electric field distribution for each layer

Similarly, the electric field strength along 4 lines on the

**Table. 4** The meshing results for three meshes

| Mesh | $N_i$ | $f_i$ ($E_{max}$) |
|---|---|---|
| 1 (fine) | 5549647 | 1.65 kV/mm |
| 2(medium) | 3593328 | 1.73 kV/mm |
| 3 (coarse) | 2415781 | 2.17 kV/mm |

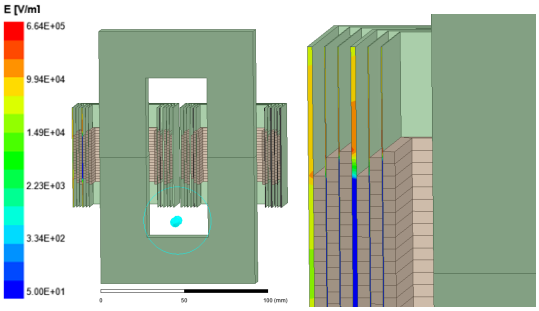


**Fig. 8** The electric field distribution in the section of the insulation

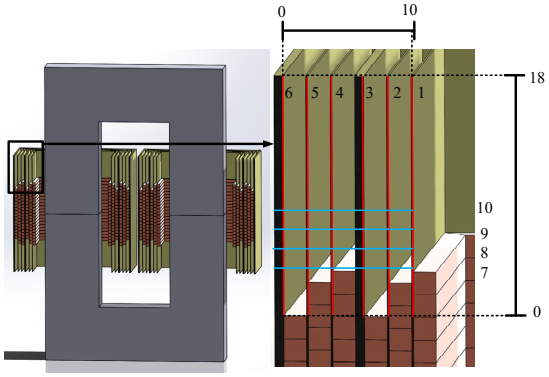


**Fig. 9** The diagram of the lines

section of the insulation is also investigated and shown in Fig. 11. It is found that near the ends of the windings, the electric field strength of each layer varies considerably, and the electric field strengths of the 1st, the 3rd, and the 4th layers are significantly greater than that of the other layers along line 1. The further away from the end of the windings, the smaller the difference in the electric field strength for each layer of insulation. This is because the electric field distribution near the end of the windings is significantly affected by the structure of the windings. As the distance between the insulation and the end of the windings increases, the effect of the windings structure on the electric field distribution decreases, and the electric field distribution in the insulation tends to become more uniform.

In summary, each layer of the insulation withstands greater electrical stress near the ends of the windings. The 1st layer of the insulation withstands the highest electrical stress near the end of the windings, which means that it is more prone to degradation and breakdown, and requires extra attention when designing the insulation system of the HVHF transformer.

## 6 Theoretical verifications

To verify the accuracy of the proposed model, the grid convergence index (GCI) method is employed in this research. The GCI method could evaluate the discretization error and check if the developed mesh is sufficiently refined in an objective way, which is popular in computational fluid dynamics (CFD) [13]. The theoretical study is conducted based on three meshes (coarse, medium, and fine). The GCI is defined as (8)-(11) [14]

**Table. 5** Theoretical verification results

| $GCI_{1,2}$(%) | $GCI_{2,3}$(%) | $r^p GCI_{12}/GCI_{23}$ |
|---|---|---|
| 1.37 | 7.14 | 1.05 |

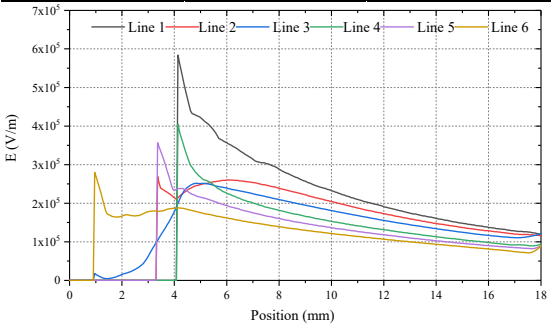


**Fig. 10** The electric field strength distribution along the lines on the surfaces

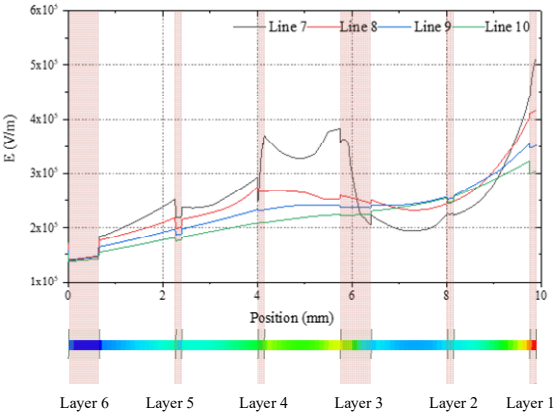


**Fig. 11** The electric field strength distribution along the lines on the section

$$\varepsilon = \frac{f_1 - f_2}{f_1} \tag{8}$$

$$r = \left(\frac{N_1}{N_2}\right)^{\frac{1}{D}} \tag{9}$$

$$p = \frac{\mathrm{In}\left(\frac{f_3 - f_2}{f_2 - f_1}\right)}{\mathrm{In}(r)} \tag{10}$$

$$GCI = \frac{F_s |\varepsilon|}{r^p - 1} 100\% \tag{11}$$

where $\mathcal{E}$ is the quantity that defines the relative difference between sequent solutions, $f$ is the quantity that represents the calculation result that characterizes the response of the system, in this research, it is the maximum electric field strength for the insulation of the HVHF transformer. $r$ is the effective grid refinement ratio, $N_i$ is the total number of grid points used for the $i$-th grid; $D$ is the dimension of the domain, $P$ is the order of convergence, $F_s$ is a safety factor.

The meshing results for three meshes are shown in Table. 4. To ensure that all calculations $f_i$ within the asymptotic convergence range, it needs to be checked by comparing whether GCIs calculated from three meshes satisfy $r^p GCI_{12}=GCI_{23}$. The theoretical verification results of the proposed model using the GCI method are shown in Table. 5. The results show that all calculations within the asymptotic convergence range and the numerical error of the model based on the fine mesh is 1.37%, which verified the accuracy of the simulation.

## 7. Conclusion

In this paper, the transient electric field for a 60 kHz HVHF transformer in a DAB DC-DC converter is established with the circuit-field coupling method. The 3-D FEM analysis of the HVHF transformer is carried out to evaluate the electrical stress suffered from the solid insulation considering the converter containing it. The electric field inside and along the surfaces of the insulation is analyzed in detail. The GCI method is applied to verify the accuracy of the proposed model. The results show that the 1st layer of the insulation withstands the highest electrical stress, with the maximum magnitude values of 1.65 kV/mm and 1.25 kV/mm inside and on the surfaces of the insulation respectively. The maximum magnetic field strength appears at the location close to the ends of the windings. At different moments in a period, each layer of the insulation presents a similar distribution characteristic. The electric field strength decreases from the position near the ends of the windings towards the ends of the insulation, and the difference between the 6 layers of the insulation decreases as the distance between the insulation and the windings increases. The structure of the windings has a considerable influence on the electric field distribution of the insulation. This paper proposed a feasible method for the HVHF transformer to evaluate electrical characteristics and identify the electrical stresses withstood by the insulation considering the converter containing it. This method could be further used to calculate the overvoltage capacity of the HVHF transformer for various power electronics applications. This model also serves as the key step for building the digital twin model of the HVHF transformer for monitoring the aging period of the insulation. Future research will focus on embedding the transient electric field model with the magnetic-thermal model into the DT model of the HVHF transformer to monitor the electro-thermal stresses withstood by the insulation.

## 8. References


[1] Olowu, Temitayo O., et al. "Multiphysics and multiobjective design optimization of high-frequency transformers for solid-state transformer applications." *IEEE Transactions on Industry Applications* 57.1 (2020): 1014-1023.

[2] Ho, Godwin Kwun Yuan, Yaoran Fang, and Bryan MH Pong. "A multiphysics design and optimization method for air-core planar transformers in high-frequency LLC resonant converters." *IEEE Transactions on Industrial Electronics* 67.2 (2019): 1605-1614.

[3] Mogorovic, Marko, and Drazen Dujic. "Sensitivity analysis of medium-frequency transformer designs for solid-state transformers." *IEEE Transactions on Power Electronics* 34.9 (2018): 8356-8367.

[4] Mi, Yan, et al. "Electrothermal aging characteristics of epoxy resin under bipolar exponential decay pulse voltage and its insulation life evaluation based on Cole-Cole model." *IEEE Transactions on Dielectrics and Electrical Insulation* 26.3 (2019): 784-791.

[5] Jahangiri, Tohid, et al. "Electric field and potential distribution in a 420 kV novel unibody composite cross-arm." *Proceedings of the Nordic Insulation Symposium*. No. 24. 2015.

[6] Lesniewska, Elzbieta Ewa, and Jan Olak. "Improvement of the insulation system of unconventional combined instrument transformer using 3-d electric-field analysis." *IEEE transactions on power delivery* 33.6 (2017): 2582-2589.

[7] Jia, Junran, et al. "Electric Field Distribution in SF 6 Gas of Converter Transformer Bushing Under Complex Voltages." *2020 IEEE International Conference on High Voltage Engineering and Application (ICHVE)*. IEEE, 2020.

[8] Liang-xian, Zhang, et al. "Research on transient electric field distribution of converter transformer valve side winding under polarity reversal." *2013 Annual Report Conference on Electrical Insulation and Dielectric Phenomena*. IEEE, 2013.

[9] Zhang, Sheng, et al. "Insulation structure design and electric field simulation of 500 kV isolation energy supply transformer for HVDC breaker." *High Voltage* (2021).

[10] Du, Boxue, et al. "Temperature dependent electric field distribution in ±800 kV valve-side bushing insulation for a converter transformer." *High Voltage* 6.1 (2020): 106-115.

[11] Chen, Bin, Xu Liang, and Nina Wan. "Design methodology for inductor-integrated litz-wired high-power medium-frequency transformer with the nanocrystalline core material for isolated DC-link stage of solid-state transformer." *IEEE Transactions on Power Electronics* 35.11 (2020): 11557-11573.

[12] Kuffel, John, and E Kuffel. *High voltage engineering fundamentals*. Elsevier, 2000.

[13] Roy, Christopher J. "Review of code and solution verification procedures for computational simulation." *Journal of Computational Physics* 205.1 (2005): 131-156.

[14] Heris, S. Zeinali, S. Gh Etemad, and M. Nasr Esfahany. "Experimental investigation of oxide nanofluids laminar flow convective heat transfer." *International communications in heat and mass transfer* 33.4 (2006): 529-535.